Effect of inhomogeneties and substrate on the dynamics of the metal-insulator transition in VO_2 thin films

M. Rodriguez-Vega,[1] M. T. Simons,[1] E. Radue,[1] S. Kittiwatanakul,[2] J. Lu,[2] S. A. Wolf,[3,2] R. A. Lukaszew,[1] I. Novikova,[1] and E. Rossi[1]

[1]*Department of Physics College of William and Mary Williamsburg VA, 23187*
[2]*Department of Material Science University of Virginia Charlottesville VA, 22904*
[3]*Department of Physics University of Virginia Charlottesville VA, 22904*

(Dated: April 24, 2015)

We study the thermal relaxation dynamics of VO_2 films after the ultrafast photo-induced metal-insulator transition for two VO_2 film samples grown on Al_2O_3 and TiO_2 substrates. We find two orders of magnitude difference in the recovery time (a few ns for the VO_2/Al_2O_3 sample vs. hundreds of ns for theVO_2/TiO_2 sample). We present a theoretical model that accurately describes the MIT thermal properties and interpret the experimental measurements. We obtain quantitative results that show how the microstructure of the VO_2 film and the thermal conductivity of the interface between the VO_2 film and the substrate affect long time-scale recovery dynamics. We also obtain a simple analytic relationship between the recovery time-scale and some of the film parameters.

I. INTRODUCTION

Vanadium dioxide (VO_2) undergoes a metal-insulator transition (MIT) around room temperature[1–3], enabling a wide range of potential applications. It has recently been demonstrated that the MIT can also be induced electrically and optically. In fact, great progress has been made in this direction in recent years: experiments have shown that is possible to photo-induce the MIT in VO_2 in the sub-picosecond timescale[4–10]. This finding makes VO_2 a material of great interest for electronic and photonic applications, such as ultra-fast switches or transistors. The realization of VO_2-based switches requires the ability to control the VO_2 MIT dynamics using external fields, as well as a better understanding of the recovery mechanisms after the external field is turned off and the material returns to its normal state. The mechanism by which the photo-induced MIT takes place in VO_2 is still not fully understood due to the complexity of the electronic behavior of VO_2 arising from the presence of strong electron-lattice coupling and electron-electron interactions. As a result, VO_2 is a unique material of great fundamental and practical interest.

At low temperatures ($T \lesssim 340$ K) the VO_2 lattice has a monoclinic structure, whereas at high temperatures ($T \gtrsim 340$ K) it has a tetragonal structure. This difference in lattice structure is reflected in the band structure: VO_2 is an insulator in the monoclinic phase and a metal in the tetragonal phase. This simple picture is complicated by the fact that in VO_2 electron-electron correlations are very strong and can provide an important contribution to the localization of the electronic states via the Mott mechanism[11–13]. It appears that a full account of the MIT must take into account the interplay of the lattice dynamics and the electron dynamics driven by strong electron-electron correlations. This is a fascinating and extremely challenging problem that in addition is complicated by the unavoidable presence of inhomogeneities[14], and the short timescale dynamics have been investigated in previous reports[15–23].

In this work, using a combined theoretical and experimental approach, we focus on the role played by inhomogeneities and the substrate in determining the relaxation dynamics of the photo-induced MIT in VO_2 films. Using a pump-probe experimental arrangement, we investigated the time evolution of the optical properties after a photo-induced MIT in VO_2 films grown under identical conditions on two different substrates, sapphire (Al_2O_3) and rutile (TiO_2). We found more than two orders of magnitude difference in the thermal relaxation rate, as shown in Fig. 1. We show that such a significant difference cannot be explained solely by the differences in the substrate thermal conductivity, and requires taking into account both structural differences in the two films and the thermal properties of the interface between the film and the substrate.

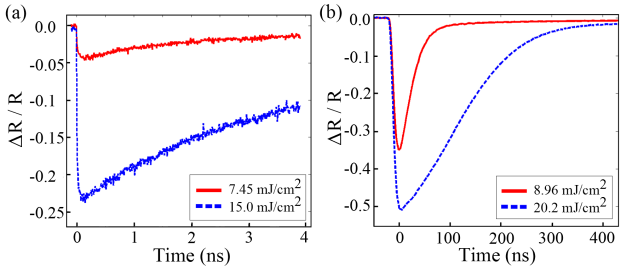

FIG. 1. Relative change in reflectivity ($\Delta R/R$) for the VO_2 film on (a) Al_2O_3 substrate and (b) TiO_2 substrate as a function of time after the MIT is induced at time $t = 0$ by a strong ultrafast pump pulse. The values of the pump fluence are shown in the legend, and the sample temperature is set to 311 K in (a) and 280 K in (b), which correspond to approximately 30 K below the critical temperature T_c for thermally-induced MIT for each sample.

We present a theoretical model that illustrates that both spatial inhomogeneities in the VO_2 films and the thermal properties of the film-substrate interface play an

important role in the thermal relaxation dynamics. We also demonstrate that such model is capable of describing the experimental results with good accuracy in a wide range of the pump laser fluences and sample temperatures. Thus, our experimental and theoretical findings are directly relevant to understanding the effect of inhomogeneities and different substrates and interfaces in the physics of the VO_2 MIT. In addition, our work is also relevant to the more general problem of how spatial inhomogeneities affect a first order phase transition. The ability of our treatment to contribute to this general problem relies on the fact that in VO_2 the two phases across the first-order transition have very different electronic properties (metallic vs. insulating behavior) that allows us to get an accurate phase mapping, via optical reflectivity measurement, of the time evolution of the metallic (insulating) fraction and, indirectly, of the spatial inhomogeneities present during the transition.

The work is organized as follows. Sec. II describes the experimental arrangements to measure the optical reflectivity time-evolution. The details of the theoretical model that we use to characterize the distribution of the films's inhomogeneities using thermally induced MIT and the long-time dynamics of the reflectivity after a photo-induced MIT are presented in Secs. III and IV, respectively. In Sec. V we demonstrate how the variations in statistical properties of the two films result in significant difference in the relaxation timescales, and in Sec. VI we provide our conclusions.

II. EXPERIMENTAL SETUP

In our experiments we studied two VO_2 thin-film samples, both of which were produced using reactive-bias target ion beam deposition (RBTIBD)[24]. One sample was grown on 0.5 mm thick c-Al_2O_3, and the thickness of the VO_2 film was 80 nm. The other sample was grown on a 0.5 mm thick TiO_2 (011) substrate, and was measured to be 110 nm thick. XRD evaluation of both films showed them to be crystalline, and detailed characterization information is available in previous reports[25,26].

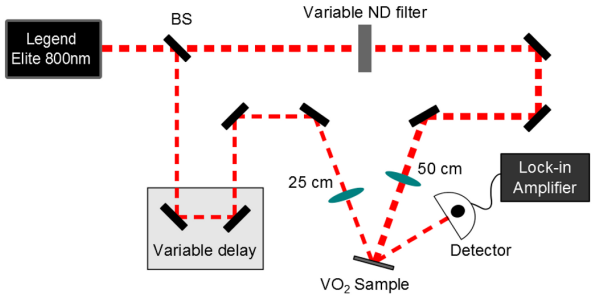

FIG. 2. Schematic of the ultrafast pump-probe setup. BS is an 80/20 beam splitter.

For the photoinduced MIT experiments we used an ultrafast laser system (Coherent Mantis oscillator and Legend Elite regenerative amplifier) with approximately 100 fs pulses with a central wavelength at 800 nm and a repetition rate of 1 kHz. The properly attenuated output of the laser was split into strong pump pulses and weaker probe pulses using a beam splitter in a standard pump-probe configuration, shown in Fig. 2. The more powerful pump beam, focused to a 180 μm diameter spot on the surface of the sample, was used to induce the MIT, and its fluence was controlled using a variable neutral-density filter (VF). The fluence of the probe beam was further attenuated to a value well below the MIT threshold ($\phi_{\text{probe}} \leq 100\ \mu\text{J/cm}^2$), and we used its reflectivity from the sample to monitor the instantaneous optical properties of the VO_2 film. The probe pulses were directed along a variable delay stage to accurately control the relative timing between the pump and probe pulses by up to 4 ns with a few fs precision. The probe beam was focused on the sample at the same spot as the pump beam, using a shorter focal length lens. When tuned to the center of the pump beam focal spot, the smaller probe beam diameter (90 μm) ensured to probe a region of uniform pump intensity.

The reflected probe power was measured using a silicon photodetector, and further analyzed using a lock-in amplifier. To minimize the effects of probe pulse instabilities, as well as long-terms drifts due to environmental changes, we report the relative change in probe reflection $\Delta R/R$ with the pump beam on or off.

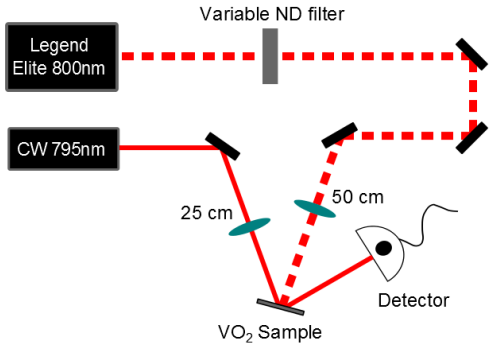

FIG. 3. Schematic of the experimental setup using a continuous-wave probe laser.

Notably the MIT relaxation of the VO_2/TiO_2 sample was not measurable with the femtosecond probe, as its characteristic decay time exceeded the 4 ns maximum pulse separation, determined by the length of the delay stage. To measure the relaxation of the metallic VO_2 grown on the rutile sample we modified our experimental setup by replacing the femtosecond probe pulses with a continuous-wave (CW) diode laser operating at 785 nm and a fast photodiode (measured response time of approximately 10 ns), as shown in Fig. 3. This detection method allowed us to measure changes in reflectivity for times longer than ≈ 20 ns after MIT, that were inacces-

sible with the femtosecond probe arrangement.

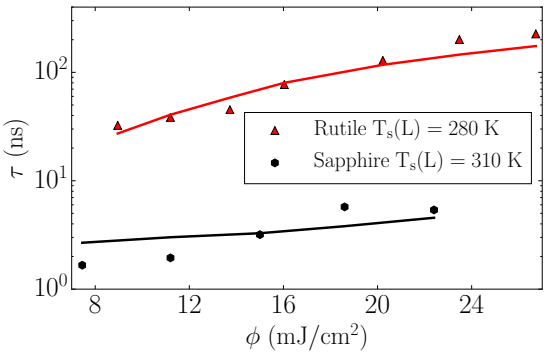

FIG. 4. Dependence of metal state decay constant τ on the laser pump fluence and substrate temperature. Dots represent experimental data, and lines corresponds to the results of the theoretical calculations. The initial temperature T_s for both sample substrates was approximately 30 K below their respective MIT critical temperatures.

Figure 1 shows sample measurements of both the VO_2/Al_2O_3 and VO_2/TiO_2 films, using the femtosceond and CW probe arrangements respectively. The analysis of the relative reflectivity for both VO_2 samples demonstrate that after the initial rapid change during the ultrafast MIT, its time evolution during relaxation is well fitted by a single exponential function with a recovery time constant τ:

$$R_{\rm fit}(t) = A(1 - e^{-t/\tau}). \qquad (1)$$

The results of such measurements are shown in Fig. 4: for VO_2/Al_2O_3 films we obtained values of τ of the order of few nanoseconds, whereas it took the VO_2/TiO_2 sample a few hundred nanoseconds to relax back to the insulating state. This two orders of magnitude difference in the recovery times was even more surprising considering that the characteristic times for the transition itself were quite similar, as demonstrated in previous studies[15]. In the discussion below we demonstrate that the relaxation dynamics strongly depend on the microstructure of the VO_2 films which in turn is strongly influenced by the properties of the substrate and their interface.

Figure 4 also reveals that the rate of thermal relaxation for both samples increases with higher pump power. This is an intuitively expected trend: since there is a significant light absorption in the VO_2 thin films, more energy must be dissipated for the case of a more powerful pump pulse. Moreover, for the higher pump powers we observed deviation of the measured reflectivity from a simple exponential recovery. The observed "flattening" of the curves is due to the pump pulse heating the sample to a temperature above the threshold value for the thermally-induced MIT. In this case reflectivity stays unchanged at the level corresponding to a fully metallic phase until the sample cools down to the transition temperature. For all experimental curves only the later exponential part of the measured reflectivity was included into the fitting thermal relaxation time analysis.

III. THEORETICAL MODELING OF NON-HOMOGENEITY IN A VO_2 THIN FILM

In order to take into account the effect of the inhomogeneities on the MIT dynamics the first step it to characterize them. Theoretical and experimental evidence[27] indicates that for thin films the probability distribution $P(D)$ of the grain size D typically follows a log-normal distribution

$$P(D) = \frac{1}{\sqrt{2\pi}\sigma D} \exp\left[-\frac{\left[\ln D/\hat{D}\right]^2}{2\sigma^2}\right]. \qquad (2)$$

In Eq. (2) D is the effective diameter of a grain assumed spherical, $\hat{D}$ is the grain size (diameter) such that $\ln \hat{D} = \langle \ln D \rangle$, where angle brackets denote averaged quantities, and σ is the standard deviation of $\ln(D)$. We note that we have also considered the case of non-spherical grains, like ellipsoids or cylinder; these cases, however, require introduction of additional fitting parameters that are not well constrained experimentally and therefore weaken the strength of the theoretical model.

Direct surface imaging experiments of the VO_2 films provides an order of magnitude of the grain size but cannot be used to quantitatively determine the parameters $\hat{D}$ and σ since they do not yield information related to variation of grain sizes across the thickness of the film. For this reason we use instead the reflectivity profile as a function of temperature through a thermally induced MIT on the same thin film sample to indirectly asses the non-homogeneity distribution function $P(D)$, as shown in Figure 5.

The temperature driven MIT in VO_2 is a first-order transition. In the ideal case its properties, such as electrical resistivity or optical reflectivity, are expected to exhibit a finite, step-like change at the critical temperature T_c, at which the sample goes from a low-temperature insulating state to a high-temperature metallic state. In thin films, however, the optical reflectivity smoothly changes from the value corresponding to the insulating phase ($R_{\rm ins}$) to the value characteristic to the metallic phase $R_{\rm m}$ as the temperature increases, as Fig. 5 illustrates. The fact that the MIT takes place over a range of temperatures implies that different regions of the sample have different T_c values. Notice that this is different from the statement, obvious for a first order transition, that metallic regions coexist with insulating regions. One natural explanation of the fact that different regions have different values of T_c is that the film is comprised of grains of different size, D, and therefore with different T_c[28,29]. The simplest, physically justified, relation between D and

T_c[30,31] is

$$T_c = T_c^{(\mathrm{bulk})}\left(1 - \frac{1}{D/D_0}\right), \quad (3)$$

where $T_c^{(\mathrm{bulk})}$ is the bulk transition temperature and D_0 is the grain diameter below which the metallic (rutile) and insulating (monoclinic) phases are indistinguishable for a given probe[29]. In general, the T_c of a grain will be affected also by the local strain experienced by the grain[32]. We note that for the purpose of calculating the time evolution of the reflectivity after the photo-induced MIT it is sufficient to know the probability distribution of T_c. In this respect Eqs. (3), (2), can be interpreted simply as effective, physically justified, equations to obtain $P(T_c)$:

$$P(T_c) = P(D(T_c))\frac{dD}{dT_c}. \quad (4)$$

In the remainder we take D_0 to be the diameter of a sphere with a volume equal to the volume of 8 VO_2 unit cells in the rutile phase, and we use the effective critical temperature $T_c = 355$ K, which is the temperature at which the VO_2/Al_2O_3 sample is completely metallic. This value is somewhat different from the the bulk VO_2, $T_c^{(\mathrm{bulk})} = 340$ K due to film strain[28,33]. The knowledge of $P(T_c)$ allows us to calculate the insulating fraction of the film (η_I) for any value of the temperature T, and therefore the metallic fraction is $\eta_M = 1 - \eta_I$:

$$\eta_I(T) = \int_T^\infty P(T_c)dT_c. \quad (5)$$

To obtain the variation of the film reflectivity R with temperature across the MIT, we use an effective medium theory (EMT)[34–37]. In EMT an inhomogenous system is replaced by an effective homogenous medium having the same, bulk, electric properties. Let ϵ_M, ϵ_I be the dielectric constants (at the probing frequency) of VO_2 in the metallic and insulating phase respectively. Then, the dielectric constant of the effective medium ϵ_{EMT} is given by the following equation:

$$\frac{\eta_I(\epsilon_I - \epsilon_{EMT})}{\epsilon_{EMT} + g(\epsilon_I - \epsilon_{EMT})} + \frac{\eta_M(\epsilon_M - \epsilon_{EMT})}{\epsilon_{EMT} + g(\epsilon_M - \epsilon_{EMT})} = 0. \quad (6)$$

In Eq. (6) g is a factor that depends on the shape of the grain. Approximating the inhomogenous film as an effective 3D composite with compact spherical inclusions we used $g = 1/3$. Let n and k be the real and imaginary parts respectively of the index of refraction, so that for the effective medium $n + ik = \sqrt{\epsilon_{EMT}}$ and therefore

$$R = \left|\frac{\cos\theta_0 - \sqrt{(n+ik)^2 - \sin^2\theta_0}}{\cos\theta_0 + \sqrt{(n+ik)^2 - \sin^2\theta_0}}\right|^2, \quad (7)$$

where θ_0 corresponds to the probe incidence angle. Using Eqs. (2)-(7), knowing ϵ_M and ϵ_I we can obtain the evolution of the $R(T)$ across the thermally induced MIT. By fitting the theoretically obtained profiles of $R(T)$ to the experimental ones we can then identify the values of the parameters $\hat{D}$, and σ_D that characterize the inhomogenous film microstructure.

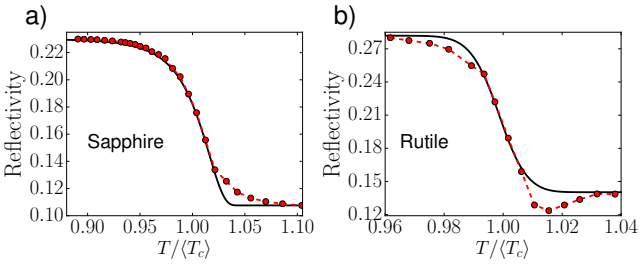

FIG. 5. Evolution of the reflectivity across thermally induced MIT for case of sapphire and rutile substrate normalized to the average critical transition temperature. For rutile substrate $\langle T_c\rangle = 314.0$ K, and for the sapphire substrate $\langle T_c\rangle = 340.1$ K.

Figures 5 (a), (b) show the evolution as a function of temperature of the reflectivity across the thermally induced MIT for a VO_2 film grown on sapphire and TiO_2, respectively. Dots connected by dashed lines show the experimental measurements, while the solid lines show the results obtained using the theoretical approach described above.

To determine the parameters entering the theory we first set the value of the imaginary part of the complex index of refraction k_M, k_I for the metallic and insulating VO_2 films to the measured values, consistent with the values reported in the literature[38,39]. Then we use Eq. (7), that relates the complex index of refraction, and optical reflectivity R, and the measured experimental value of R_I (R_M) at the insulating (metallic) phase to fix the corresponding values of the real part of the complex index of refraction n_I (n_M), and therefore obtain the dielectric constants ϵ_I, ϵ_M entering Eq. (6). Using Eq. (5), $\eta_M = (1 - \eta_I)$, and Eq. (6) we can then obtain ϵ_{EMT}, and therefore the value of the effective medium reflectivity using Eq. (7), across the thermally induced MIT. By fitting the profile of $R(T)$ to the experimental data for the case of VO_2 on sapphire we obtain that the average grain size, and the standard deviation, that determine the probability distribution $P(D)$ are $\langle D\rangle = 64.7$ nm and $\sigma_D = 38.5$ nm, respectively. For the case of VO_2 on TiO_2 we obtain $\langle D\rangle = 17.4$ nm and $\sigma_D = 1.1$ nm. These results show that the average grain size is of the same order in the two type of VO_2 films, VO_2/Al_2O_3 and VO_2/TiO_2. On the other hand, the standard deviation of the grain size is almost an order of magnitude different: VO_2/TiO_2 samples appear to have a much smaller variation in the grain size than VO_2/Al_2O_3 samples. This is also reflected in the distribution of T_c. Figures 6 (a), (b) show the probability distributions $P(D)$ corresponding to the values of $\langle D\rangle$ and σ_D used to obtain the good theoretical fit to the evolution of $R(T)$ shown in Fig. 5.

Figures 6 (c), (d) show the corresponding probability distribution for T_c. With knowledge of $P(D)$ the theoretical

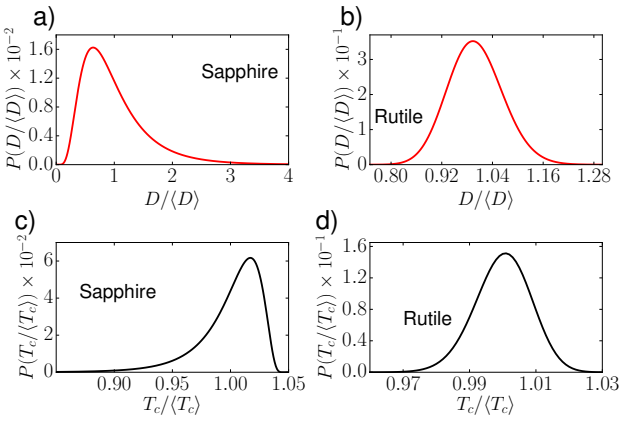

FIG. 6. Panels (a) and (b) show the grain size probability distributions normalized to the average grain size for sapphire ($\langle D\rangle = 64.7$ nm) and rutile ($\langle D\rangle = 17.4$ nm) substrate respectively. Panels (c) and (d) show the critical temperature probability distribution normalized to the average critical temperature for sapphire ($\langle T_c\rangle = 340.1$ K) and rutile ($\langle T_c\rangle = 314.0$ K) respectively. The bulk critical temperature is taken to be $T_c^{(bulk)} = 355$ K.

model also allows us to obtain the temperature evolution of the insulating and metallic fraction of the VO_2 film across the thermally induced MIT. The results for the case of VO_2 on sapphire and TiO_2 are shown in Figures 7 (a), (b) respectively. The much smaller value of σ_D for VO_2/TiO_2 compared to VO_2/Al_2O_3 is reflected in a much steeper variation of η_I, and therefore of $R(T)$, across the MIT.

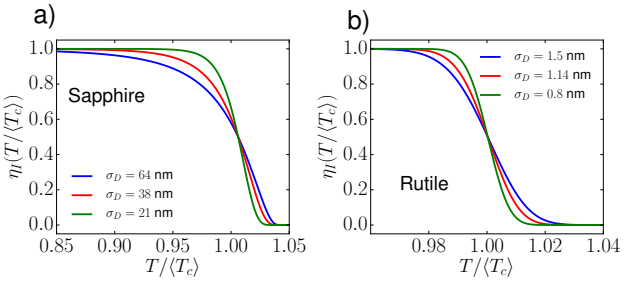

FIG. 7. Evolution of the insulating partial volume η_I across the thermally induced MIT for case of (a) sapphire and (b) rutile substrates. For rutile, $\langle T_c\rangle = 314.0$ K, and for sapphire $\langle T_c\rangle = 340.1$ K.

IV. THEORETICAL MODELING OF THE RELAXATION DYNAMICS OF THE MIT

In this section we show that the proposed treatment of the inhomogeneous VO_2 films can also accurately describe their thermal relaxation at long-time scales after the photo-induced MIT, when the dynamics of the VO_2 film can be assumed to be adiabatic. In this regime the film cools by transferring heat to the substrate. In the process of cooling more and more metallic regions become insulating and therefore cause a significant change in reflectivity.

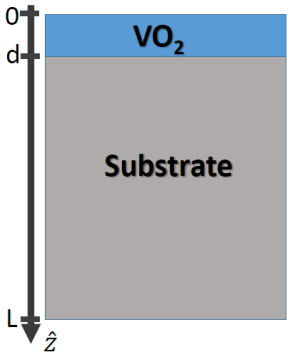

FIG. 8. Sketch of the heterostructure considered in this work. It is composed of a vanadium dioxide (VO_2) thin-film deposited on top of a substrate. The substrates considered in this work are titanium dioxide (TiO_2), and aluminum oxide (Al_2O_3). For VO_2/TiO_2 $d = 110$ nm while for VO_2/Al_2O_3 $d = 80$ nm. For both substrates, $L = 0.5$ mm.

In our experiment the VO_2 films have a thickness d equal to or smaller than 110 nm (see Fig. 8), which is comparable with the laser $1/e$ penetration depth $\delta \simeq 110 - 130$ nm[15]. Thus, we can assume that the pump pulse heats the film uniformly throughout its thickness. To describe the heat transfer process between the film and the substrate, we assume the temperature to be uniform throughout the film for all times. Effectively, given this conditions, the heat transfer problem becomes a one-dimensional problem, and the equation for the rate of change of the heat (Q) in the film takes the form:

$$\frac{dQ}{dt} = A \times d \times (\rho_I C_I \eta_I(T_f) + \rho_M C_M \eta_M(T_f) + L(T_f)\tilde{P}(T_f)\rho_{av}) \frac{\partial T_f}{\partial t} , \quad (8)$$

where T_f is the film temperature, A is the area of the film, ρ_I (ρ_M) is the density in the insulating (metallic) phase, $\rho_{av} \equiv (\rho_I + \rho_M)/2$, C_I (C_M) is the heat capacity in the insulating (metallic) phase, L is the specific heat and $P(T_f)dT_f$ is the fraction of the sample undergoing the MIT in the time interval dt during which the film temperature is in the interval $[T_f, T_f + dT_f]$. In analogy to T_c, we assume

$$L = L^{(\text{bulk})} \left(1 - \frac{1}{D/D_0}\right) , \quad (9)$$

where $L^{(\text{bulk})}$ is the value of the specific heat for bulk VO_2. For a given T_f, the values of $\eta_M(T_f)$ and $\eta_I(T_f)$ are obtained using the method previously described, having

fixed the parameters characterizing $P(D)$ via the results for the thermally induced MIT.

The rate of change of heat in the film given by Eq. (8) must be equal to the heat current (J_Q) across the interface between the film and the substrate:

$$J_Q = -\sigma_K A(T_f - T_s(d)) \tag{10}$$

where σ_K is the Kapitza constant characterizing the thermal conductivity of the interfaces[40–43], and $T_s(d)$ is the temperature of the substrate at the surface facing the VO_2 film. Combining Eq. (8) and Eq. (10), for T_f we obtain the equation:

$$\Big[\rho_I C_I \eta_I(T_f) + \rho_M C_M \eta_M(T_f) + L(T_f)\tilde{P}(T_f)\rho_{av}\Big]\frac{\partial T_f}{\partial t} = -\frac{\sigma_K}{d}(T_f - T_s(d)). \tag{11}$$

Notice that equation (11) is highly nonlinear due to the T_f-dependence of the terms within the square brackets on the left hand side.

The temperature distribution within the substrate, $T_s(z,t)$, satisfies the diffusion equation:

$$\frac{\partial T_s(z,t)}{\partial t} = \frac{k_s}{C_s \rho_s}\frac{\partial^2 T_s(z,t)}{\partial z^2} \tag{12}$$

where k_s, C_S, ρ_s are the thermal conductivity, heat capacity, and mass density, respectively, of the substrate. The bottom of the substrate, for which $z = L$ (see Fig. 8), is kept at a fixed temperature $T_s(L)$. At the film/substrate interface the heat transferred from the film must be equal to the heat current $k_s \partial T_s/\partial z|_{z=d}$. We then have that the boundary conditions completing Eq. (12) are:

$$T_s(z = L, t) = T_s^{(B)}; \tag{13}$$

$$k_s \left.\frac{\partial T_s(z,t)}{\partial z}\right|_{z=d} = -\sigma_K(T_f(t) - T_s(z = d, t)). \tag{14}$$

Equations (11)-(14), combined with knowledge of the probability distribution $P(D)$, and relations (3), (9), completely define the temperature evolution of the VO_2 film. While these equations can in general be solved only numerically, some qualitative understanding of the decay time τ can be gained if we make some simplifications. Let us assume first that the critical temperature probability distribution is well approximated by a Gaussian profile $\tilde{P}(T_c) = 1/(\sqrt{2\pi}\sigma_{T_c})\exp\{-(T_c - \langle T_c\rangle)^2/(2\sigma_{T_c}^2)\}$, as it is the case for the VO_2 sample grown on rutile (see Fig. (6d)). In this case, the insulating volume fraction is simply given by $\eta_I(T) = \frac{1}{2}\left[1 - \mathrm{erf}\left((T - \langle T_c\rangle)/(\sqrt{2}\sigma_{T_c})\right)\right]$. Then assuming that the pump pulse is strong enough to drive the entire film into a fully metallic state at $t = 0$, the time-dependence of the insulating volume fraction can be approximated by a simple exponential form $\eta_I(t) = 1 - Ae^{-t/\tau}$. In this case, an expression for the temperature can be obtained through the relationship $\eta_I(T(t)) = \eta_I(t)$. Furthermore, assuming that the substrate temperature T_s does not change with time, and that the latent heat L is temperature-independent, we can calculate the decay constant τ:

$$\tau = Cd\frac{\sigma_{T_c}}{\sigma_K}\frac{\Big(C_M\rho_M + L\rho_{av}\tilde{P}(T_0)\Big)}{T_0 - T_s} + \tau_0\ , \tag{15}$$

where the constant $C > 0$, and τ_0 can only be determined by solving the full system of equations (11)-(13)

It is interesting to note that despite its many limitations, Eq.(15) captures many important qualitative traits of the actual relaxation process. For example, Figure (9) shows a plot of the decay constant as a function of σ_{T_c} obtained solving the full system of equations (11)-(13) for two different values of the average critical temperature, and same initial temperature $T_0 = 360$ K. It is easy to see that the decay time τ follows the linear trend predicted by Eq. (15) in the limit $(T_0 - \langle T_c\rangle) \gg \sqrt{2}\sigma_{T_c}$. Similarly, an exact solution shows the inverse dependence of τ on the Kapitza constant, $\tau \propto \sigma_K^{-1}$, as shown in Figure 10.

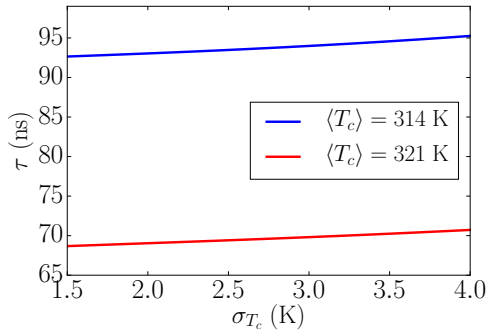

FIG. 9. Full numerical calculation of the dependence of metal state decay constant τ on σ_{T_c} for two different values of the sample average critical temperature $\langle T_c\rangle$, and $T_s(L) = 280$ K. The initial temperature $T_0 = 360$ K is such that the sample is initially fully metallic, and $(T_0 - \langle T_c\rangle)/(\sqrt{2}\sigma_{T_c}) \approx 9$.

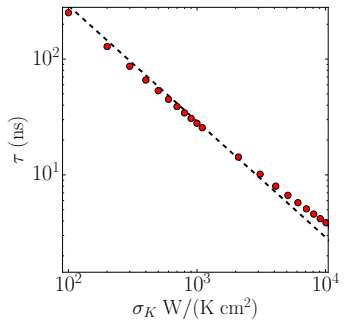

FIG. 10. VO_2/Al_2O_3 metal state decay time τ dependence on the Kapitza constant σ_k for $\langle D\rangle = 64.7$ nm, $\sigma_D = 38.5$ nm, substrate temperature $T_s(L) = 310$ K, and fluence $\phi = 8$ mJ/cm^2. The red dots correspond to numerical calculations, and the dashed line is given by $\tau \propto \sigma_K^{-1}$

VO_2 heat capacity insulating phase C_I [44]	0.656 J/(g K)
heat capacity metallic phase C_M [44]	0.78 J/(g K)
density insulating phase ρ_I [43]	4.57 g/cm^3
density metallic phase ρ_M [43]	4.65 g/cm^3
thermal conductivity insulating phase κ_I [45]	3.5 W/(m K)
thermal conductivity metallic phase κ_M [45]	6 W/(m K)
bulk latent heat $L^{(Bulk)}$ [44]	51.8 J/g
TiO_2 heat capacity C_s [46]	0.686 J/(g K)
density ρ_s [43]	4.25 g/cm^3
thermal conductivity κ_s [47]	8 W/(m K)
Al_2O_3 heat capacity C_s [48]	0.779 J/(g K)
density ρ_s [48]	3.98 g/cm^3
thermal conductivity κ_s [48]	30 W/(m K)
VO_2/TiO_2 absortion coefficient at 800 nm α [15]	0.01 nm^{-1}
VO_2/Al_2O_3 absortion coefficient at 800 nm α [15]	0.0076 nm^{-1}

TABLE I. Parameters of VO_2 and substrates.

	VO_2/TiO_2	VO_2/Al_2O_3
$\langle D\rangle$	17.4 nm	64.7 nm
σ_D	1.1 nm	38.5 nm
$\langle T_c\rangle$	314.0 K	340.1 K
σ_{T_c}	2.6 K	8.8K
$n_M + ik_M$	$1.53 + i0.8$	$1.49 + i0.65$
R_M	0.14	0.11
$n_I + ik_I$	$3.03 + i0.57$	$2.60 + i0.60$
R_I	0.28	0.23

TABLE II. Comparative table between VO_2/TiO_2, and VO_2/Al_2O_3 sample parameters.

V. EFFECT OF INHOMOGENEITIES ON THE RELAXATION DYNAMICS OF THE PHOTO-INDUCED MIT

Using the theoretical approach described in Sec. IV we can obtain the time evolution of the optical reflectivity R through the MIT, as well as explain the significant difference in relaxation timescales between the two VO_2 samples considered. In all the numerical calculations we assume C_I, ρ_I, C_M, ρ_M to be equal to the bulk value for insulating and metallic VO_2, see Table I. The initial film temperature is fixed by the pump fluence taking into account the gaussian profile of the pulse and the fact that some of the heat is lost by the film during the time interval $[0, t_0]$ for which our analysis does not apply, $t = 0$ is time at which the pump pulse hits the VO_2 film and $t_0 = 10$ ns for VO_2/TiO_2 films and $t_0 = 0.5$ ns for VO_2/Al_2O_3 films.

Considering that we have identified the parameters in both samples that determine $P(D)$ using the profiles of $R(T)$ for the thermally induced MIT, the only undetermined parameter entering the theory is the Kapitza constant σ_K. This last step can be done by analyzing the experimentally measured time evolution of the optical reflectivity for different laser fluences and substrate temperatures, shown in Fig. 11 for the VO_2/TiO_2 sample. It is easy to see that all experimental curves are well approximated assuming the same value for the Kapitza constant $\sigma_K = 1100$ W/(K cm^2).

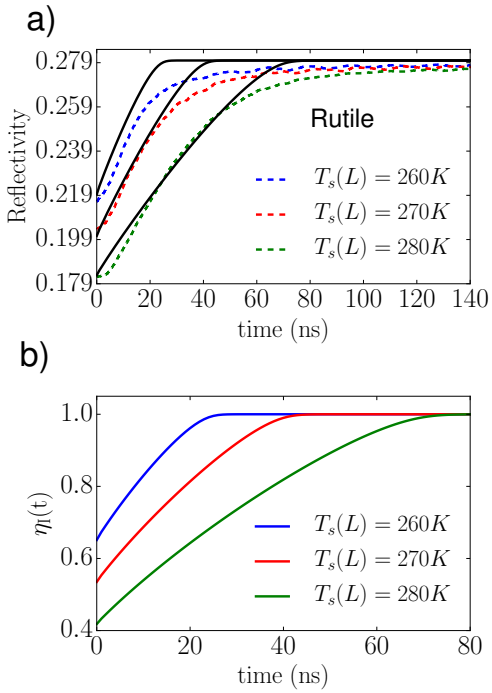

FIG. 11. (a) Time evolution of reflectivity after the photo-induced MIT for VO_2/TiO_2 for three different $T_s(L)$ and $\phi = 9$ mJ/cm^2. The solid curves correspond to the theoretical results, and the dashed curves correspond to the experimental results. For the three theory curves we use $\sigma_K = 1100$ W/(K cm^2). Panel (b) shows the corresponding insulating fraction time evolution.

To understand the origin of the large difference between the recovery time scale VO_2/TiO_2 films and VO_2/Al_2O_3 films, we first consider the effect of the average and standard deviation of the grain size. The theoretical calculations predict that inhomogineities in the film can play an important role. For example, Fig. 12 shows the calculated dependence of the decay constants τ on the grain size standard deviation σ_D for two values of $\langle \ln D\rangle$, as defined in Eq. (2). Broader distributions correspond to larger time scales. At the same time differences in $\langle D\rangle$ and σ_D between VO_2/Al_2O_3 and VO_2/TiO_2 films alone cannot explain the observed differences in the recovery times of $R(t)$ for the two films. To illustrate this, we model the time evolution of $R(t)$ after the photo-induced MIT in the VO_2/Al_2O_3 film using the grain distribution parameters $\langle D\rangle$ and σ_D obtained by fitting the corresponding $R(T)$ curve, but using the value of the Kapitza constant, obtained for the

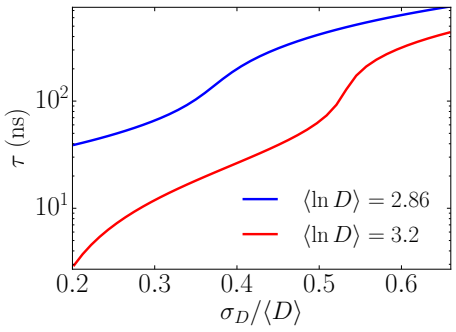

FIG. 12. Dependence of the VO_2/TiO_2 metal state decay time constant τ on σ_D for two values of $\langle \ln D \rangle$, as defined in Eq. (2), Kapitza constant $\sigma_K = 1100$ W/(K cm^2), substrate temperature $T_s(L) = 280$ K, and initial fluence $\phi = 9$ mJ/cm^2.

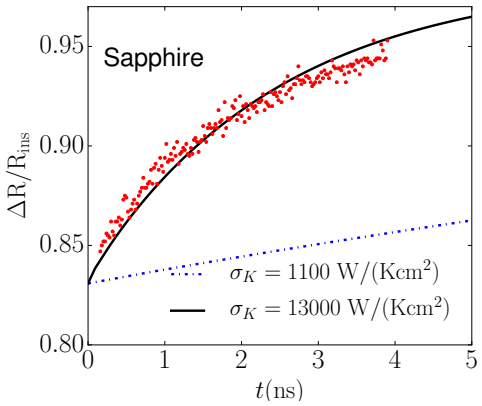

FIG. 13. VO_2/Al_2O_3 reflectivity time evolution after photo-induced MIT for $\phi = 7.5$ mJ/cm^2. The red dots correspond to the experimental result. The dotted curve correspond to the theory with $\sigma_K = 1100$ W/(K cm^2), and the solid curve corresponds to $\sigma_K = 13000$ W/(K cm^2).

VO_2/TiO_2 sample $\sigma_K = 1100$ W/(K cm^2). The results of these calculations are shown as a dashed curve in Fig. 13. It is evident that the large difference in the values of τ must be due to a significant difference in σ_K between the two films. Indeed, the experimental curves $R(t)$ for VO_2/Al_2O_3 are well approximated by the theoretical results assuming $\sigma_K = 13,000$ W/(K cm^2), shown as a solid curve in Fig. 13.

Figure 14 shows the time evolution of the VO_2 film and substrate temperatures (close to the interface) for the VO_2/Al_2O_3 film, panel (a), and for the VO_2/TiO_2 film, panel (b), using the parameter values summarized in Table I. It helps to qualitatively understand the differences in thermal relaxation between two samples. Due to lower values of Kapitza constant and thermal conductivity, thermal energy stays more concentrated near the VO_2-TiO_2 interface, keeping the temperature of the VO_2 film above T_c longer.

To investigate the temperature dependence of the

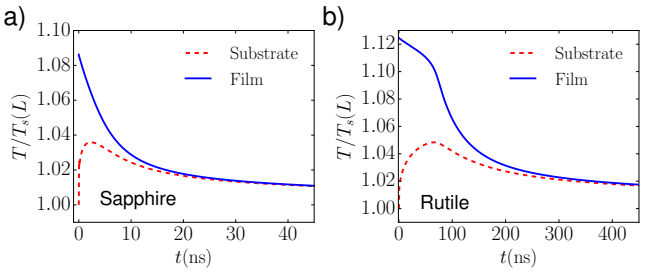

FIG. 14. Film and substrate temperature time evolution. For sapphire (a), $T_s(L) = 310$ K, and for rutile (b), $T_s(L) = 280$ K.

thermal relaxation we repeated the measurements while changing the base substrate temperature of the VO_2/TiO_2 sample. For these measurements the sample was placed inside a cryostat, and cooled down to temperatures $T_s(L)$ between 260 K and 298 K. Since the VO_2 relaxation is due to the thermal exchange with the substrate, we expect that lowering the substrate temperature should lead to faster relaxation. The results of these measurements, along with the theoretical calculations, are shown in Figure 15. We again observe a good semiquantitative agreement between theoretical and experimental results. Also, note that the simple expression for the decay constant τ Eq. (15) captures the overall decay rate drop at lower substrate temperatures $T_s(L)$. It is worth pointing out that all the theoretical curves are obtained using the fixed set of parameters shown in Table I.

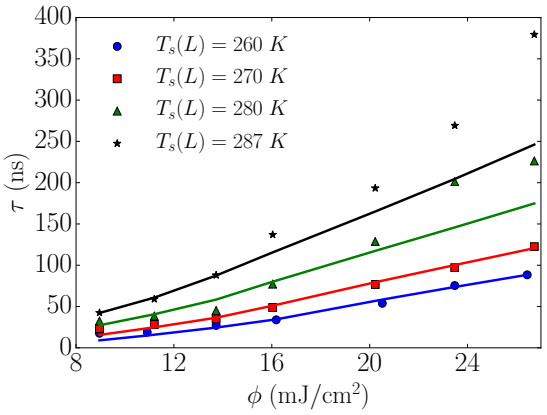

FIG. 15. Dependence of metal state decay constant τ on fluence and substrate temperature for VO_2/TiO_2.

An important advantage of the presented theoretical model is that it allows an accurate description of the relaxation dynamics of different VO_2 films under a wide range of experimental conditions using a single set of parameters describing the inhomogenous distribution of grains in each film and the thermodynamic constants for the film-substrate interface. For example, Fig. 4 shows an excellent agreement between the experimental mea-

surements and theoretical calculations across the entire range of pump laser fluences, limited on the lower end by our ability to reliably detect the variation in the probe reflectivity, and on the upper end by the damage threshold of our sample (pump fluence > 40 mJ/cm^2).

VI. CONCLUSIONS

In conclusion, we have presented a combined experimental and theoretical study of the long time-scale recovery dynamics of VO_2 films following an ultrafast photo-induced metal-insulator transition. We have presented a theoretical approach to describe the time evolution of the dielectric constant of VO_2 films though the MIT, and therefore of the reflectivity, over long-time scales after a photo-induced metal insulator transition. We also have shown how the parameters characterizing the grain size distribution and the thermal conductivity of the interface between the film and substrate affect such evolution. The theory presented can be generalized to describe the dynamics (in the adiabatic limit) across a first order phase transition of other inhomogeneous systems. By comparing theoretical and experimental results we have been able to determine the relevant parameters characterizing the VO_2 films and the thermal conductivity of the interface and attribute the large difference in the recovery time scale between VO_2/TiO_2 and VO_2/Al_2O_3 films to a large difference in the thermal conductivity of the interface. These results might be important for technological application of VO_2 based on its ability to change phase at temperatures close to room temperature.

VII. ACKNOWLEDGMENTS

This work was funded in part by NSF, DMR-1006013: Plasmon Resonances and Metal Insulator Transitions in Highly Correlated Thin Film Systems, Jeffress Trust Awards program in Interdisciplinary Research, ONR-N00014-13-1-0321, and the NASA Virginia Space Grant Consortium. We also acknowledge support from the NRI/SRC sponsored ViNC center and the Commonwealth of Virginia through the Virginia Micro-Electronics Consortium (VMEC).

[1] N. Mott, *Metal-insulator transitions* (1998).
[2] F. J. Morin, Phys. Rev. Lett. **3**, 34 (1959).
[3] M. Imada, A. Fujimori, and Y. Tokura, Reviews of Modern Physics **70**, 1039 (1998).
[4] A. Cavalleri and D. V. D. Linde, Applied Physics A **579**, 577 (1999).
[5] A. Cavalleri, C. Tóth, C. Siders, J. Squier, F. Ráksi, P. Forget, and J. Kieffer, Physical Review Letters **87**, 237401 (2001).
[6] A. Cavalleri, T. Dekorsy, H. Chong, J. Kieffer, and R. Schoenlein, Physical Review B **70**, 3 (2004).
[7] A. Cavalleri, M. Rini, H. Chong, S. Fourmaux, T. Glover, P. Heimann, J. Kieffer, and R. Schoenlein, Physical Review Letters **95**, 067405 (2005).
[8] H.-T. Kim, Y.-W. Lee, B.-J. Kim, B.-G. Chae, S. J. Yun, K.-Y. Kang, K.-J. Han, K.-J. Yee, and Y.-S. Lim, Physical Review Letters **97**, 4 (2006).
[9] M. Nakajima, N. Takubo, Z. Hiroi, Y. Ueda, and T. Suemoto, Journal of Luminescence **129**, 1802 (2009).
[10] T. L. Cocker, L. V. Titova, S. Fourmaux, H. C. Bandulet, D. Brassard, J. C. Kieffer, M. A. El Khakani, and F. A. Hegmann, Applied Physics Letters **97**, 221905 (2010).
[11] A. Zylbersztejn and N. F. Mott, Phys. Rev. B **11**, 4383 (1975).
[12] D. Paquet and P. Leroux-Hugon, Phys. Rev. B **22**, 5284 (1980).
[13] G. Stefanovich, A. Pergament, and D. Stefanovich, Journal of Physics: Condensed Matter **12**, 8837 (2000).
[14] M. M. Qazilbash, M. Brehm, B. G. Chae, P. C. Ho, G. O. Andreev, B. J. Kim, S. J. Yun, A. V. Balatsky, M. B. Maple, F. Keilmann, et al., Science **318**, 1750 (2007).
[15] E. Radue, L. Wang, S. Kittiwatanakul, J. Lu, S. A. Wolf, E. Rossi, R. A. Lukaszew, and I. Novikova, Journal of Optics **17**, 025503 (2015).
[16] T. L. Cocker, L. V. Titova, S. Fourmaux, G. Holloway, H.-C. Bandulet, D. Brassard, J.-C. Kieffer, M. A. El Khakani, and F. A. Hegmann, Physical Review B **85**, 155120 (2012).
[17] M. F. Becker, A. B. Buckman, R. M. Walser, T. Lpine, P. Georges, and A. Brun, Applied Physics Letters **65**, 1507 (1994).
[18] H.-T. Kim, Y. W. Lee, B.-J. Kim, B.-G. Chae, S. J. Yun, K.-Y. Kang, K.-J. Han, K.-J. Yee, and Y.-S. Lim, Phys. Rev. Lett. **97**, 266401 (2006).
[19] M. Rini, Z. Hao, R. W. Schoenlein, C. Giannetti, F. Parmigiani, S. Fourmaux, J. C. Kieffer, A. Fujimori, M. Onoda, S. Wall, et al., Applied Physics Letters **92** (2008).
[20] C. Kübler, H. Ehrke, R. Huber, R. Lopez, A. Halabica, R. Haglund, and A. Leitenstorfer, Physical Review Letters **99**, 116401 (2007).
[21] D. J. Hilton, R. P. Prasankumar, S. Fourmaux, A. Cavalleri, D. Brassard, M. A. El Khakani, J. C. Kieffer, A. J. Taylor, and R. D. Averitt, Phys. Rev. Lett. **99**, 226401 (2007).
[22] A. Pashkin, C. Kübler, H. Ehrke, R. Lopez, A. Halabica, R. F. Haglund, R. Huber, and A. Leitenstorfer, Physical Review B **83**, 195120 (2011).
[23] E. Abreu, M. Liu, J. Lu, K. G. West, S. Kittiwatanakul, W. Yin, S. A. Wolf, and R. D. Averitt, New Journal of Physics **14**, 083026 (2012).
[24] K. G. West, J. Lu, J. Yu, D. Kirkwood, W. Chen, Y. Pei, J. Claassen, and S. a. Wolf, Journal of Vacuum Science & Technology A: Vacuum, Surfaces, and Films **26**, 133 (2008).
[25] L. Wang, E. Radue, S. Kittiwatanakul, C. Clavero, J. Lu, S. a. Wolf, I. Novikova, and R. a. Lukaszew, Optics letters **37**, 4335 (2012).
[26] E. Radue, E. Crisman, L. Wang, S. Kittiwatanakul, J. Lu, S. A. Wolf, R. Wincheski, R. A. Lukaszew, and I. Novikova,

Journal of Applied Physics **113**, 233104 (2013).
[27] C. G. Granqvist and R. A. Buhrman, Journal of Applied Physics **47**, 2200 (1976).
[28] R. Aliev, V. Andreev, V. Kapralova, V. Klimov, A. Sobolev, and E. Shadrin, Physics of the Solid State **48**, 929 (2006).
[29] L. Wang, I. Novikova, J. M. Klopf, S. Madaras, G. P. Williams, E. Madaras, J. Lu, S. A. Wolf, and R. A. Lukaszew, Advanced Optical Materials **2**, 30 (2014).
[30] Q. Jiang, J. Li, and B. Chi, Chemical Physics Letters **366** (2002).
[31] M. Zhang, M. Y. Efremov, F. Schiettekatte, E. A. Olson, A. T. Kwan, S. L. Lai, T. Wisleder, J. E. Greene, and L. H. Allen, Phys. Rev. B **62**, 10548 (2000).
[32] M. K. Liu, M. Wagner, E. Abreu, S. Kittiwatanakul, a. McLeod, Z. Fei, M. Goldflam, S. Dai, M. M. Fogler, J. Lu, et al., Physical Review Letters **111**, 096602 (2013).
[33] D. Brassard, S. Fourmaux, M. Jean-Jacques, J. C. Kieffer, and M. A. El Khakani, Applied Physics Letters **87**, 051910 (2005).
[34] D. Bruggeman, Annalen der Physik **24**, 636 (1935).
[35] R. Landauer, J. Appl. Phys. **23**, 779 (1952).
[36] X. C. Zeng, D. J. Bergman, P. M. Hui, and D. Stroud, Phys. Rev. B **38**, 10970 (1988).
[37] E. Rossi, S. Adam, and S. D. Sarma, Phys. Rev. B **79**, 245423 (2009).
[38] H. W. Verleur, A. S. Barker Jr, and C. N. Berglund, Physical Review **172**, 788 (1968).
[39] J. Kana Kana, J. Ndjaka, G. Vignaud, a. Gibaud, and M. Maaza, Optics Communications **284**, 807 (2011).
[40] P. L. Kapitza, J. Phys. USSR **4** (1941).
[41] G. L. Pollack, Reviews of Modern Physics **41**, 48 (1969).
[42] R. Stoner and H. Maris, Physical review. B, Condensed matter **48**, 16373 (1993).
[43] H. Wen, L. Guo, E. Barnes, J. H. Lee, D. A. Walko, R. D. Schaller, J. A. Moyer, R. Misra, Y. Li, E. M. Dufresne, et al., Phys. Rev. B **88**, 165424 (2013).
[44] C. N. Berglund and H. J. Guggenheim, Phys. Rev. **185**, 1022 (1969).
[45] D.-W. Oh, C. Ko, S. Ramanathan, and D. G. Cahill, Applied Physics Letters **96**, 151906 (2010).
[46] D. de Ligny, P. Richet, E. F. W. Jr, and J. Roux, Physics and Chemistry of Minerals **29**, 267 (2002).
[47] W. R. Thurber and A. J. H. Mante, Phys. Rev. **139**, A1655 (1965).
[48] V. Pishchik, L. a. Lytvynov, and E. R. Dobrovinskaya, *Sapphire: Material, Manufacturing, Applications* (Springer US, 2009), 1st ed., ISBN 978-0-387-85694-0.